Astronomy & Astrophysics manuscript no. HighPrecisionParameters
February 5, 2024

Letter to the Editor

Double Red Giant Branch and Red Clump features of Galactic disc stellar populations with Gaia *GSP-Spec*

Alejandra Recio-Blanco[1], P. de Laverny[1], P. A. Palicio[1], S. Cassisi[2,3], A. Pietrinferni[2], and N. Lagarde[4]

[1] *Université Côte d'Azur, Observatoire de la Côte d'Azur, CNRS, Laboratoire Lagrange, Bd de l'Observatoire, CS 34229, 06304 Nice cedex 4, France*
e-mail: alejandra.recio-blanco@oca.eu
[2] *INAF – Osservatorio Astronomico di Abruzzo, Via M. Maggini s/n, I-64100 Teramo, Italy*
[3] *INFN, Sezione di Pisa, Largo Pontecorvo 3, 56127 Pisa, Italy*
[4] *Laboratoire d'Astrophysique de Bordeaux, Université Bordeaux, CNRS, B18N, Allée Geoffroy Saint-Hilaire, 33615 Pessac, France*

Received ; accepted

ABSTRACT

Context. The bimodality of the Milky Way disc, in the form of a thick short disc and a thinner more radially extended one, encrypts the complex internal evolution of our Galaxy and its interaction with the environment.
Aims. To disentangle the different competing physical processes at play in Galactic evolution, a detailed chrono-chemical-kinematical, and dynamical characterisation of the disc bimodality is necessary, including high number statistics.
Methods. Here we make use of an extremely precise subsample of the Gaia DR3 *GSP-Spec* catalogue of stellar chemo-physical parameters. The selected database is composed of 408 800 stars with a median uncertainty of 10 K, 0.03 and 0.01 dex in $T_{\rm eff}$, $\log(g)$ and [M/H], respectively.
Results. The stellar parameter precision allows to break the age-metallicity degeneracy of disc stars. For the first time, the disc bimodality in the Kiel diagramme of giant stars is observed, getting rid of interstellar absorption issues. This bimodality produces double Red Giant Branch sequences and Red Clump features for mono-metallicity populations. A comparison with BaSTI isochrones allows to demonstrate that an age gap is needed to explain the evolutionary sequences separation, in agreement with previous age-metallicity relations obtained using Main-Sequence Turn Off stars. A bimodal distribution in the stellar mass-[α/Fe] plane is observed at constant metallicity. Finally, a selection of stars with [M/H]=0.45±0.03 dex shows that the most metal-rich population in the Milky Way disc presents an important proportion of stars with ages in the range 5-13 Gyr. This old, extremely metal-rich population is possibly a mix of migrated stars from the internal Galactic regions, and old disc stars formed before the last major merger of the Milky Way.
Conclusions. The Gaia *GSP-Spec* Kiel diagrammes of disc mono-abundance stellar populations reveal a complex, non linear age-metallicity relation crafted by internal and external processes of Galactic evolution. Their detailed analysis opens new opportunities to reconstruct the puzzle of the Milky Way disc bimodality.

Key words. tbd

1. Introduction

The structure of the Milky Way disc is known to be bimodal since the seminal works of Yoshii (1982) and Gilmore & Reid (1983). It is composed of a thick, more primitive stellar population, and of a thin more radially extended component, containing stars, gas and dust. The disc bimodality encrypts crucial information about the physical processes of our Galaxy formation, as it is the result of more than 10 Gyr of evolution. It emerges from the complex interplay of internal evolutionary processes and the interaction of our Milky Way with its ecosystem. As a consequence, a variety of physical mechanisms are invoked to explain the spatial, kinematical, dynamical and chemical properties of the thick and the thin discs, and their evolution with time. Early turbulence (Bournaud et al. 2009), radial migration (e.g Schönrich & Binney 2009b; Minchev & Famaey 2010; Trick et al. 2019; Prantzos et al. 2023), gas infall (eg Spitoni et al. 2023a), galaxy mergers (eg. Abadi et al. 2003; Renaud et al. 2021) and disc marginal stabilty (Park et al. 2021), can be cited among the numerous studied processes and their related literature.

From the observational point of view, characterizing the disc bimodality implies precise data and high number statistics. For this reason, the thick/thin disc transition has been at the core of the observational strategy of all recent spectroscopic surveys of the Milky Way. In particular, the existent correlations between chemical abundances and kinematical and/or dynamical properties have been explored inside the Solar neighbourhood, using HARPS and GALAH data, among others (e.g. Adibekyan et al. 2013; Santos-Peral et al. 2021; Hayden et al. 2020) and outside the Solar neighbourhood, using for instance Gaia-ESO Survey, APOGEE or Gaia *GSP-Spec* data (e.g. Recio-Blanco et al. 2014; Hayden et al. 2015; Gaia Collaboration et al. 2023a). Thick disc stellar populations are kinematically hotter than thin disc ones. Additional evidence of disc bimodality comes

from chemical abundance ratios. In particular, the thick and thin disc populations define two parallel sequences in the [α/Fe] abundance vs. metallicity plane, with thick disc stars presenting higher [α/Fe] ratios than thin disc stars of similar [M/H], with a gap in [α/Fe] whose detailed properties indeed depend on the specific α-element taken into consideration(Prantzos et al. 2023). The two sequences seem to merge in the super-Solar metallicity regime, although this fact is observationally challenging to confirm due to the complex analysis of metal-rich stellar spectra (Santos-Peral et al. 2020). Moreover, the temporal evolution of the disc chemical properties suggests the existence of two ditinct phases in the age-metallicity relation (e.g. Haywood et al. 2013; Hayden et al. 2017; Santos-Peral et al. 2021; Lagarde et al. 2021; Miglio et al. 2021; Xiang & Rix 2022). In the metal-intermediate regime, a gap of about 2-5 Gyr between mono-metallicity populations of the thick and the thin disc seems to be present. Conversely, a gap in metallicity of about 0.5 dex at the start of the thin disc formation 7-9 Gyr ago is detected. This metallicity gap is progressively reduced, and seems to disappear 4-5 Gyr ago. The relative proportion of thin to thick disc stars is linked to the different structural properties of the two discs, with the thick disc having a shorter scale-length and a larger scale-height than the thin one.

To disentangle the Galactic disc dichotomy, and in particular, its temporal evolution, the study of large samples of stars in a large spatial volume is mandatory. To this purpose, giant stars are ideal tracers of disc populations up to very large distances. However, their use is hampered by a severe age-metallicity degeneracy of their physical properties (in particular colour and therefore effective temperature), and non negligible uncertainties on interstellar absorption in the Galactic plane. In this letter, we use an extremely precise sample of stellar chemo-physical parameters (cf. Sect. 2) from the Gaia DR3 (Gaia Collaboration et al. 2023b) *GSP-Spec* catalogue (Recio-Blanco et al. 2023), to break the age-metallicity degeneracy of disc stellar populations. New constraints on disc bimodality using the $T_{\rm eff}$ vs. log(g) diagramme are presented in Sect. 3. Finally, the age distribution of extremely metal-rich stars in the disc is explored in Sect. 4. The conclusions of this Letter are summarized in Sect. 5.

2. A high precision DR3 *GSP-Spec* data set

This work makes use of the stellar physical parameters and chemical abundances derived from the *Gaia* RVS spectra by the MatisseGauguin analysis procedure (Recio-Blanco et al. 2006, 2016; Bijaoui et al. 2012) of the *GSP-Spec* module (Recio-Blanco et al. 2023). The data are available through the *astrophysical_parameters* table of the *Gaia* DR3 archive. In particular, we employ the stellar effective temperature $T_{\rm eff}$ (`teff_gspspec`), the surface gravity log(g) (`logg_gspspec`), the metallicity [M/H] (`mh_gspspec`) and the abundance of α-elements [α/Fe] and magnesium [Mg/Fe] with respect to iron (`alphafe_gspspec` and `mgfe_gspspec`, respectively). The prescriptions recommended by Recio-Blanco et al. (2023) in Tables 3 and 4 have been used to calibrate log(g), [M/H] [α/Fe] and [Mg/Fe] as a function of $T_{\rm eff}$ (see Appendix A). It is important to note that the *GSP-Spec* DR3 [M/H] abundances are indeed indicators of the [Fe/H] abundance, as iron lines dominate the non-α element features

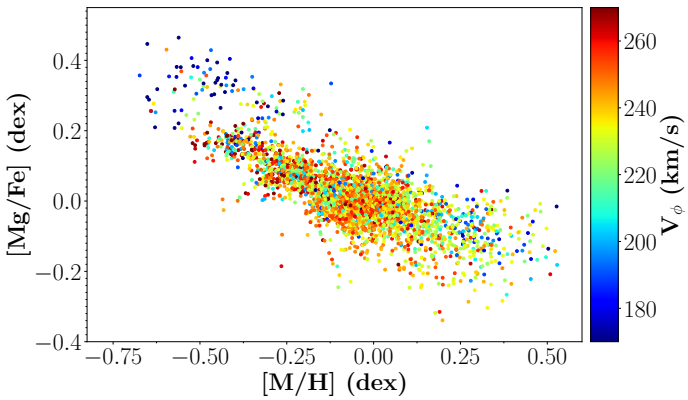

Fig. 1. Gaia *GSP-Spec* [Mg/Fe] abundances as a function of metallicity for a subsample of 3,209 stars with high SNR data, good quality flags and uncertainties in [Mg/Fe] lower than 0.05 dex. The colour code shows the Galactic azimuthal velocity.

used by *GSP-Spec* for the `mh_gspspec` estimations. As a consequence, [M/H] abundances can be directly compared to [Fe/H] values of chemical evolution models or stellar isochrones.

To select high precision parameters, our working sample contains only stars with a metallicity uncertainty defined as (`mh_gspspec_upper`-`mh_gspspec_lower`)/2, lower than 0.025 dex, and a signal-to-noise (`rv_expected_sig_to_noise`) higher than 100. Moreover, to ensure the quality of the parametrization, we imposed the following filters in the `flags_gspspec` chain (cf. Recio-Blanco et al. 2023, Table 2): the `vbroadT,G,M`, `vradT,G,M` and the `KMgiantPar` flags have been set to 0, and the `extrapol` flag to 0 or 1. Finally, to clean for the remaining less reliable solutions, we selected stars not cooler than 3750 K and with a goodness-of-fit parameter `logchisq_gspspec`<-3.7. The final sample contains 408,800 stars with a median uncertainty of 10 K, 0.03 and 0.01 dex in $T_{\rm eff}$, log(g) and [M/H] respectively. The signal-to-noise of the corresponding RVS spectra is distributed between 100 and 2823 with a median at 144. The G magnitude is distributed between 3.47 and 12.44 mag with a median at 8.8 mag. The stars are located between 6.7 kpc to 10 kpc from the Galactic centre and within 1 kpc from the Galactic plane. Finally, we have used the kinematical and orbital parameters of the selected stars computed by Palicio et al. (2023) to complement the spectroscopic *GSP-Spec* chemo-physical ones.

3. Bimodal Giant Branches and Red Clumps

A common way of separating the stellar populations in the thin and the thick discs is to use the distribution of individual abundances in the [α/Fe] vs. [Fe/H] plane. Nevertheless, the separation power of this chemical diagnostic depends on the considered α-element[1] (eg., Mikolaitis et al. 2014;

[1] Those elements whose production is dominated by Type II supernovae, as Mg, show a higher difference in their abundance with respect to iron between thin and thick disc stars at constant metallicity. The Gaia *GSP-Spec* [α/Fe] estimation is dominated by the Ca triplet (Recio-Blanco et al. 2023) and it is therefore a tracer of [Ca/Fe], which has a lower separating power between the thin and thick disc than [Mg/Fe]

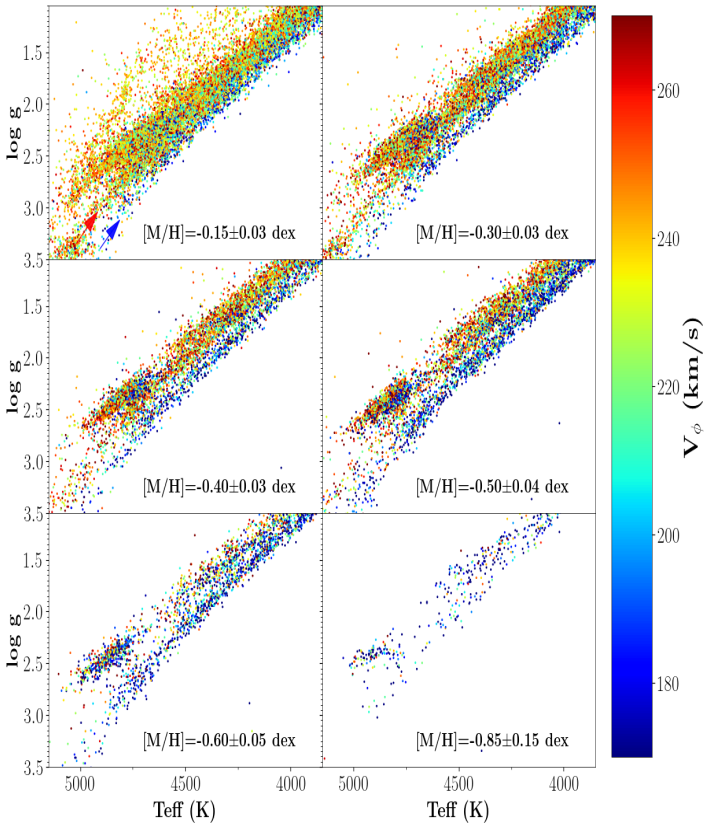

Fig. 2. Giant branch and red clump locus of the $T_{\rm eff}$ vs. log(g) diagramme in six different metallicity bins. The colour code illustrates the azimuthal Galactic velocity. Two RGBs and two red clumps are distinguishable in all the panels, with the exception of the more metal-poor one at [M/H]=-0.85 dex, in which only lower Galactic rotational velocity stars are present.

Prantzos et al. 2023). Figure 1 presents the [Mg/Fe] abundance distribution as a function of metallicity for a subsample of stars of our working data set with high-quality magnesium abundances. In particular, we have selected stars whose uncertainty in [Mg/Fe] is lower than 0.05 dex and the two corresponding Mg *GSP-Spec* quality flags are equal to zero. In addition, to avoid potential problems due to line blending, a $T_{\rm eff}$ threshold ranging between 4500 K in the metal-poor regime, and 5200 K in the metal-rich one, has been imposed. As expected, two sequences are visible in the resulting abundance distribution presented in Fig. 1. To help the identification of thin and thick disc populations, corresponding to the lower and the upper sequences respectively, the colour-code shows the Galactic azimuthal velocity of the stars.

Moreover, thanks to the high number statistics of the Gaia *GSP-Spec* catalogue, our high-precision working sample can be used to confidently select stars in narrow metallicity bins. For each bin, the upper and lower confidence values of the *GSP-Spec* metallicity indeed allow to build stellar subsamples whose [M/H] is within that bin with a probability of 70%. This metallicity selection is presented in Fig. 2, using again a colour code on the Galactic azimuthal velocity, V$_\phi$. The surface gravity versus temperature distribution of giant stars is shown, considering six separate [M/H] bins. Two different stellar evolutionary paths, highlighted by a red and a blue arrow in the upper left panel, are observed. They are separated by a gap in the $T_{\rm eff}$ vs. log(g) plane, and they are visible from the red giant branch (RGB) and the Red Clump up to the Asymptotic Giant Branch.

It can be seen in this Fig. 2 that a first evolutionary path is defined by stars with high Galactic rotational velocities, appearing in reddish colours. This population progressively fades from [M/H]=-0.15 dex (upper left panel) to [M/H]=-0.60 dex (bottom left panel), being absent in the more metal-poor bin at [M/H]=-0.85 dex (bottom right panel).

The second evolutionary path is visible in the cooler side of the first one and it is populated by stars with lower Galactic rotational velocities (bluish colours in the Figure). It progressively detaches from the high V$_\phi$ evolutionary path as metallicity diminishes, showing a separated RGB in the metal-intermediate regime. This low-V$_\phi$ population is increasingly more visible as metallicity decreases, being the only one present in the most metal-poor bin.

The gap in $T_{\rm eff}$ and/or log(g) between the two evolutionary paths of mono-metallicity populations, suggests different age distributions, with the hotter population being younger than the other one. This fact, combined with the kinematical characteristics (high Galactic rotation for the hotter population and mild Galactic rotation for the cooler one) advocates for their identification as the evolutionary loci of thin and thick disc stars, respectively. This is also supported by the dynamical characteristics of the two populations, as shown in Fig.A.2 and A.3. The cooler, high-V$_\phi$ population is observed to have orbits with higher pericentres (R$_{peri}$) and lower maximun distances from the Galactic plane (Z$_{max}$), than the hotter, lower V$_\phi$ population at a given metallicity. This is coherent with the expected orbital characteristics of the thin disc, namely a longer scale-length and a shorter scale-height with respect to the thick disc.

To further constrain the characteristics of the observed thin and thick disc bimodality in the $T_{\rm eff}$ vs. log(g) plane, Fig. 3 presents a more detailed analysis of an intermediate metallicity bin selecting stars with `mh_gspspec_lower`>-0.4 dex and `mh_gspspec_upper`<-0.3 dex. The figure is composed of nine panels zooming on different regions of the Kiel diagram and kinematically decomposing the thin and thick disc evolutionary sequences. The upper and middle row panels show the region around the RGB and the Red Clump, while the Main Sequence Turn Off region is presented in the bottom row panels. In addition, a kinematical decomposition is displayed, from left to right. No kinematical selection is made in the leftmost panels, showing all the stars in this metallicity bin. On the contrary, the middle and right column panels present the stars with thin disc or thick disc kinematics, respectively. The kinematical selection is based on the departures from the circular velocity value at the corresponding Galactic position of the star. In particular, thin disc stars in the middle panels are required to have a V$_\phi$ higher than 30 km/s with respect to their circular velocity V$_{circ}$. The thick disc population in the right panels is selected to have a V$_\phi$ lower than -60 km/s with respect to V$_{circ}$ (see for instance Lagarde et al. 2021). These criteria avoid as much as possible the overlapping regime in V$_\phi$ between the thin and the thick disc. This allows to cleanly separate the evolutionary sequences in the Kiel diagram using an independent parameter. In the different panels of Fig. 3, two RGBs and two Turn Offs

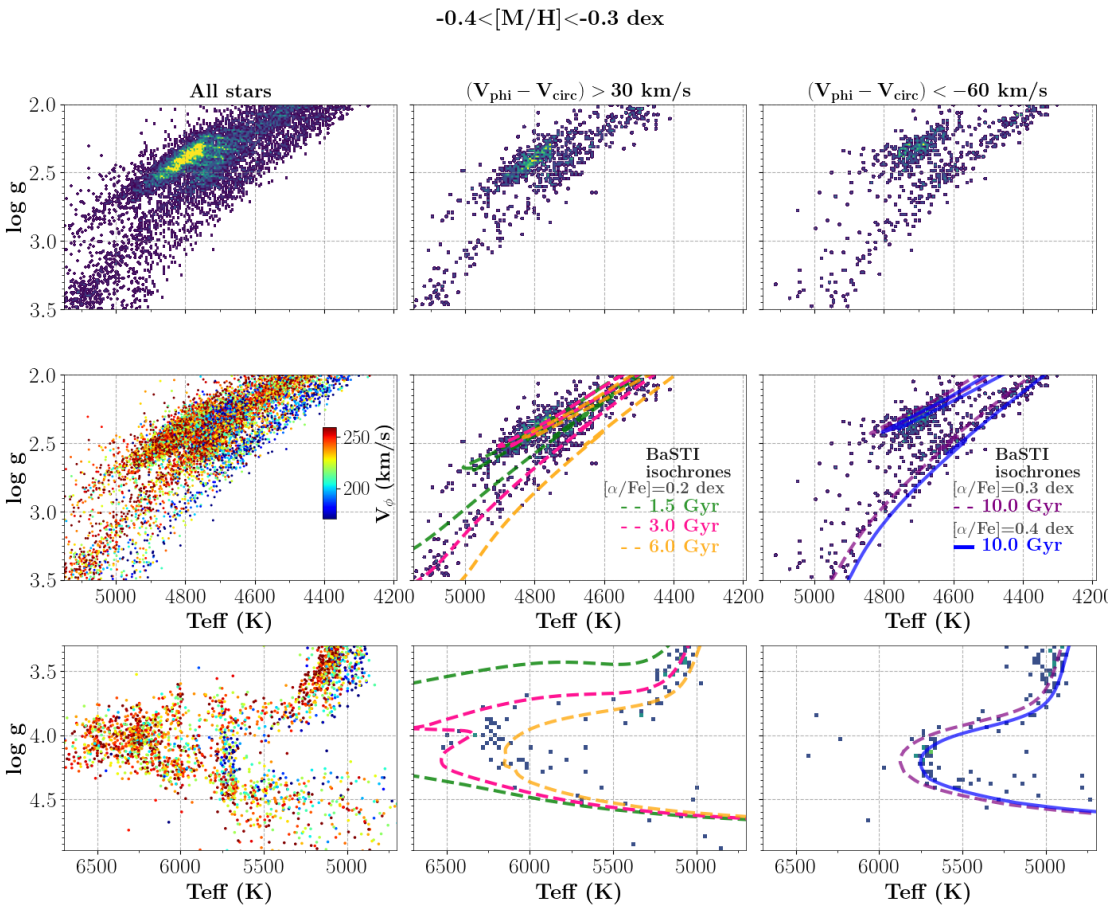

Fig. 3. Disc stellar population with [M/H]=-0.35±0.05 dex. The panels show a kinematical decomposition of the RGB and Red Clump (first and second row) and the Turn Off (bottom row) features . Left column panels show all the selected stars and present the double evolutionary sequences both for giants and dwarfs. The central and right column panels show the thin and thick disc populations, respectively, separated thanks to their V_ϕ. BaSTI isochrones with different α-enhancements are fitted to the data .

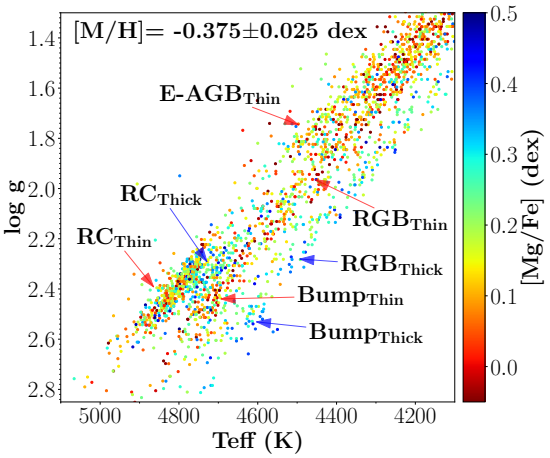

Fig. 4. $T_{\rm eff}$ vs. log(g) diagram for stars with [M/H]=-0.375±0.025 dex, using the [Mg/Fe] abundance as colour code. The main stellar evolutionary features of thin and thick disc populations can be identified.

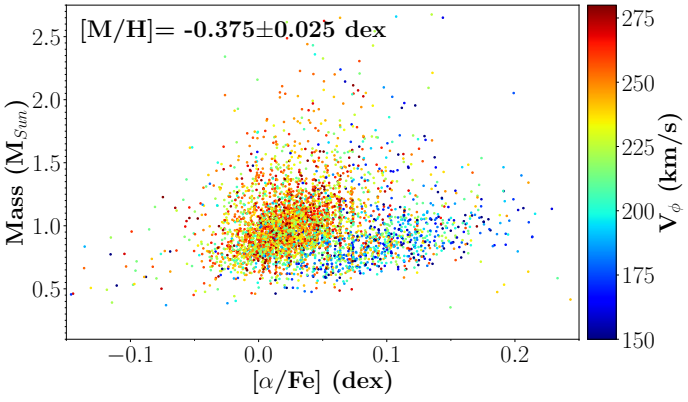

Fig. 5. Stellar mass as a function of [α/Fe] for stars with [M/H]=-0.375±0.025 dex, using the Galactic azimuthal velocity as colour code. Thick disc stars, with lower V_ϕ velocities, lower masses and higher [α/Fe], define a Mass-[α/Fe] sequence separated from thin disc stars.

separated by a small gap can be identified. In addition, two red clumps shifted in both $T_{\rm eff}$ and log(g) are observed.

Contrary to the colour-magnitude diagramme, the spectroscopic $T_{\rm eff}$ vs. log(g) plane has the advantage of being reddening free, which is particularly important for disc stars

outside the Solar Neighbourhood. As a consequence, and thanks to the *GSP-Spec* high precision in the stellar parameters of the selected stars, the age distribution of the observed two populations can be confidently retrieved through isochrone fitting. For this purpose, we adopt the BaSTI-IAC isochrone library for both solar-scaled (Hidalgo et al. 2018) and α-enhanced (Pietrinferni et al. 2021) heavy element distribution [2] and [Fe/H]=-0.35 dex (the central value of the analysed metallicity bin). On one hand, as shown in the central panel of Fig. 3, the thin disc RGB and Red Clump at this metallicity can be fitted with isochrones in the range 1.5 to 6 Gyr. This age distribution is compatible with the isochrone fit of the Turn Off populations, presented in the middle bottom panel. On the other hand, the thick disc RGB and Red Clump follow the loci of a 10 Gyr isochrone, as presented in the middle right panel. This value is again compatible with the fit of the Turn Off population in the bottom right panel. The thick disc evolutionary sequences seem to present a lower age dispersion than the thin disc ones, as expected from the tighter age-metallicity correlation of the thick disc (e.g. Haywood et al. 2013). Moreover, the fitted thick disc isochrones illustrate the effect of the [α/Fe] enrichment for the same metallicity and age. Although a shift in $T_{\rm eff}$ and $\log(g)$ is visible and should be considered for careful age determinations on a star by star basis, it is insufficient to explain the gap between the thin and thick disc evolutionary sequences at this metallicity. An age gap of about 4 Gyr is required to interpret the observed dichotomy.

To complete this study, we focus on an even narrower metallicity bin composed of 6,601 stars with [M/H]=-0.375±0.025 dex. Figure 4 presents the $T_{\rm eff}$ vs. $\log(g)$ diagramme centred on the giant stars locus and using the [Mg/Fe] abundance as colour-code. The bimodality of disc populations is present in all the different stellar evolutionary sequences along this diagrammeAs expected (cf. Fig. 1), the thin and the thick disc evolutionary sequences correspond to two different regimes of [Mg/Fe] abundance, with thick disc stars presenting higher values. Finally, we computed the masses of the stars in the above mentioned metallicity bin ([M/H]=-0.375±0.025 dex) using their *GSP-Spec* parameters and E(BP-RP) colours (see. Appendix C). Figure 5 presents the derived stellar masses as a function of the [α/Fe] abundance. The selected stars have an uncertainty lower than 0.05 $M_\odot$ in mass and 0.01 dex in [α/Fe]. The Galactic azimuthal velocity is used as a colour code. The thin and thick disc stars define again two different regimes in this plot. In particular, the population of stars typical of thick disc stars (with V_ϕ values lower than 200 km/s) has a median mass 0.1 $M_\odot$ lower than stars with higher V_ϕ values in the thin disc. This is consistent with the age difference between the two populations.

4. Super-Solar metallicity populations in the disc

The study of disc stars presenting the highest levels of metal enrichment is key to understand the mechanisms of radial migration (Sellwood & Binney 2002; Schönrich & Binney 2009a, e.g.). Figure 6 shows the Kiel diagramme for the metallicity bin [M/H]=+0.45±0.03 dex (a factor ∼3 larger than the Solar metal enrichment), and the corresponding fit of three BaSTI isochrones with 5, 8 and 13 Gyr. Rather unexpectedly, an important fraction of the stars in this extremely metal-rich regime are old. The different evolutionary features are globally well fitted by a 8 Gyr isochrone, although younger and older isochrones, in the interval of about 5 to 13 Gyr are also compatible with about 85% of the selected stars. Interestingly enough, this age interval is similar to the one observed for bulge populations by Joyce et al. (2023). Additionaly, about 15% of the stars are in the temperature regime of younger populations, with $T_{\rm eff}$ values between 6000 and 8000 K. Although the relative proportion of young to old stars is difficult to evaluate (among other things, due to a lack of completeness), the data highlight the existence of an old extremely metal-rich population. It is interesting to note that the radial distribution of stars in this metallicty bin spans from 7.5 to 9 kpc from the Galactic centre (with a median at 8.24 kpc). The distribution of maximum orbital distances from the Galactic plane, Z_{max}, ranges from 0 to 1 kpc (with a median at 0.26 kpc). Finally, the median Galactic azimuthal velocity is 235 km/s, with a dispersion of 25 km/s.

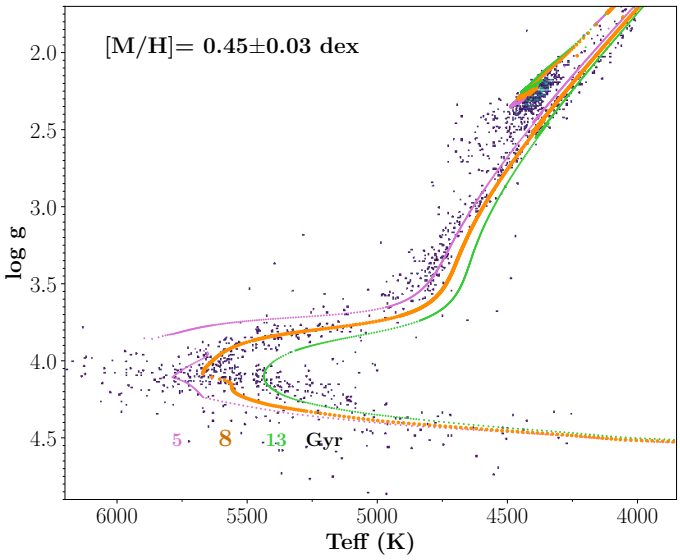

Fig. 6. Kiel diagramme of the disc extremely metal-rich population with [M/H]=+0.45±0.03 dex. Solar-scaled BaSTI isochrones of 5, 8 and 13 Gyr (pink, orange and green, respectively) are overlaid to the data.

5. Conclusions

The Gaia DR3 *GSP-Spec* catalogue allows to study the disc stellar populations in a high precision chemo-physical parameters regime, with unprecedentedly high number statistics. This opens new horizons to characterise in detail the thin and thick discs evolution outside the Solar neighbourhood, getting rid of interstellar absorption issues and breaking the age-metallicity degeneracy. In this work, we present for the first time the consequence of Galactic disc bimodality in the physical properties of its giant stars population,

[2] Since the BaSTI models are available for [α/Fe]=0.00 and +0.40, at any given [Fe/H] and age a linear interpolation in [α/Fe] has been adopted in order to derive isochrones for any requested α-element enhancement. Only a 45 K offset seems to be needed to match the BaSTI isocrones and the calibrated *GSP-Spec* data, confirming the coherence of both $T_{\rm eff}$ scales.

that is, double RGB sequences and Red Clump features for mono-metallicity populations. An age gap is needed to explain the evolutionary sequences separation, in agreement with previous age-metallicity relations using Turn Off stars (e.g. Xiang & Rix 2022) and supporting the modeling of the disc chemical evolution by distinct infall episodes (e.g. Spitoni et al. 2023b). The bimodal evolutionary sequences are characterized in kinematics, dynamics, [Mg/Fe] abundances and stellar masses consistently derived from Gaia data. Additionally, a selection of extremely metal-rich disc stars with [M/H]=0.45±0.03 dex contains a considerable proportion of very old stars (ages 5-13 Gyr) reaching distances of up to 9 kpc from the Galactic centre, and maximum orbital distances from the Galactic plane of up to 1 kpc. This old population could be composed of thin disc stars having migrated from the internal regions of the Galaxy, and thick disc stars formed before the last major merger of the Milky Way, namely that of the Gaia-Enceladus satellite about 9 yrs ago (Helmi et al. 2018; Belokurov et al. 2018; Gallart et al. 2019). The detailed analysis of precise Gaia *GSP-Spec* Kiel diagrammes of mono-abundance stellar populations opens new pathways to disentangle the complex puzzle of Galactic disc bimodality, at the core of Milky Way's evolutionary processes.

Acknowledgements. This work has made use of data from the European Space Agency (ESA) mission Gaia (https://www.cosmos.esa.int/gaia), processed by the Gaia Data Processing and Analysis Consortium (DPAC, https://www.cosmos.esa.int/web/gaia/dpac/consortium). Funding for the DPAC has been provided by national institutions, in particular the institutions participating in the Gaia Multilateral Agreement. PAP acknowledges support by the Centre National d'études Spatiales (CNES).

References

Abadi, M. G., Navarro, J. F., Steinmetz, M., & Eke, V. R. 2003, ApJ, 597, 21
Adibekyan, V. Z., Figueira, P., Santos, N. C., et al. 2013, A&A, 554, A44
Bailer-Jones, C. A. L., Rybizki, J., Fouesneau, M., Demleitner, M., & Andrae, R. 2021, AJ, 161, 147
Belokurov, V., Erkal, D., Evans, N. W., Koposov, S. E., & Deason, A. J. 2018, MNRAS, 478, 611
Bijaoui, A., Recio-Blanco, A., de Laverny, P., & Ordenovic, C. 2012, Statistical Methodology, 9, 55
Bournaud, F., Elmegreen, B. G., & Martig, M. 2009, ApJ, 707, L1
Casagrande, L., Lin, J., Rains, A. D., et al. 2021, MNRAS, 507, 2684
de Laverny, P. e. a. 2024, å
Gaia Collaboration, Recio-Blanco, A., Kordopatis, G., et al. 2023a, A&A, 674, A38
Gaia Collaboration, Vallenari, A., Brown, A. G. A., et al. 2023b, A&A, 674, A1
Gallart, C., Bernard, E. J., Brook, C. B., et al. 2019, Nature Astronomy, 3, 932
Gilmore, G. & Reid, N. 1983, MNRAS, 202, 1025
Hayden, M. R., Bland-Hawthorn, J., Sharma, S., et al. 2020, MNRAS, 493, 2952
Hayden, M. R., Bovy, J., Holtzman, J. A., et al. 2015, ApJ, 808, 132
Hayden, M. R., Recio-Blanco, A., de Laverny, P., Mikolaitis, S., & Worley, C. C. 2017, A&A, 608, L1
Haywood, M., Di Matteo, P., Lehnert, M. D., Katz, D., & Gómez, A. 2013, A&A, 560, A109
Helmi, A., Babusiaux, C., Koppelman, H. H., et al. 2018, Nature, 563, 85
Hidalgo, S. L., Pietrinferni, A., Cassisi, S., et al. 2018, ApJ, 856, 125
Joyce, M., Johnson, C. I., Marchetti, T., et al. 2023, ApJ, 946, 28
Lagarde, N., Reylé, C., Chiappini, C., et al. 2021, A&A, 654, A13
Miglio, A., Chiappini, C., Mackereth, J. T., et al. 2021, A&A, 645, A85
Mikolaitis, Š., Hill, V., Recio-Blanco, A., et al. 2014, A&A, 572, A33
Minchev, I. & Famaey, B. 2010, ApJ, 722, 112
Palicio, P. A., Recio-Blanco, A., Poggio, E., et al. 2023, A&A, 670, L7
Park, M. J., Yi, S. K., Peirani, S., et al. 2021, ApJS, 254, 2
Pietrinferni, A., Hidalgo, S., Cassisi, S., et al. 2021, ApJ, 908, 102
Prantzos, N., Abia, C., Chen, T., et al. 2023, MNRAS, 523, 2126
Recio-Blanco, A., Bijaoui, A., & de Laverny, P. 2006, MNRAS, 370, 141
Recio-Blanco, A., de Laverny, P., Allende Prieto, C., et al. 2016, A&A, 585, A93
Recio-Blanco, A., de Laverny, P., Kordopatis, G., et al. 2014, A&A, 567, A5
Recio-Blanco, A., de Laverny, P., Palicio, P. A., et al. 2023, A&A, 674, A29
Renaud, F., Agertz, O., Read, J. I., et al. 2021, MNRAS, 503, 5846
Santos-Peral, P., Recio-Blanco, A., de Laverny, P., Fernández-Alvar, E., & Ordenovic, C. 2020, A&A, 639, A140
Santos-Peral, P., Recio-Blanco, A., Kordopatis, G., Fernández-Alvar, E., & de Laverny, P. 2021, A&A, 653, A85
Schönrich, R. & Binney, J. 2009a, MNRAS, 396, 203
Schönrich, R. & Binney, J. 2009b, MNRAS, 399, 1145
Sellwood, J. A. & Binney, J. J. 2002, MNRAS, 336, 785
Spitoni, E., Recio-Blanco, A., de Laverny, P., et al. 2023a, A&A, 670, A109
Spitoni, E., Recio-Blanco, A., de Laverny, P., et al. 2023b, A&A, 670, A109
Trick, W. H., Coronado, J., & Rix, H.-W. 2019, MNRAS, 484, 3291
Xiang, M. & Rix, H.-W. 2022, Nature, 603, 599
Yoshii, Y. 1982, PASJ, 34, 365

Table A.1. Polynomial coefficients for the calibration of the *GSP-Spec* MatisseGauguin gravities, metallicities and [Mg/Fe] abundances as a function of $t = T_{\rm eff}/5750$

Parameter	p_0	p_1	p_2	p_3
$\log(g)$	-0.2320	0.8291	0.7441	-1.1677
[M/H]	1.2739	-1.1383	-1.4776	1.3398
[Mg/Fe]	-15.8586	48.1211	-48.5437	16.1383

Appendix A: Calibration of surface gravity, metallicity and magnesium abundance.

The raw *GSP-Spec* values for surface gravity, metallicity and magnesium abundance with respect to iron have been calibrated following the procedures described in Recio-Blanco et al. (2023). However, as the temperature range spanned by these data is large, it has been found to be more adapted to calibrate as a function of $T_{\rm eff}$ instead of as a function of $\log(g)$. To this purpose, and following Recio-Blanco et al. (2023), polynomial corrections in the form:

$$Param_{\rm calibrated} = Param + \sum_{i=0}^{3} p_i \cdot t^i \quad \text{(A.1)}$$

have been applied, where $Param$ is either $\log(g)$, [M/H] or [Mg/Fe]. t is the relative temperature with respect to the Sun, $T_{\rm eff}/5750$, and p_i are the corresponding polynomial coefficients from Table A.1.

Appendix B: Density diagrammes and dynamical dependencies

The thin/thick disc bimodality in the Kiel diagram illustrated for six different mono-abundance populations in Section 3 is also distinguishable in the stellar distribution in this plane (see Fig A.1). Thanks to the precision of the *GSP-Spec* chemo-physical parameters, the double RGB sequences are visible without the use of any kinematical or dynamical information, particularly in the intermediate metallicity domain.

In addition, Fig. A.2 and Fig. A.3 allow to observe the trends of the two RGB sequences with the orbital pericentre, R_{peri}, and the maximum distance from the Galactic plane, Z_{max}, respectively. The typical thin and thick disc ranges in R_{peri} and Z_{max} can be distinguished. The hotter sequence presents larger orbital pericentres and lower Z_{max} values, typical of thin disc stars. On the contrary, the cooler sequence corresponds to a population with pericentres closer to the Galactic centre and reaching larger distances from the plane, characterising thick disc stars.

Appendix C: Estimation of stellar Masses from Gaia *GSP-Spec* parameters, astrometry and photometry

Stellar masses were derived for 6,601 stars with [M/H]=-0.375±0.025 dex using their *GSP-Spec* spectroscopic atmospheric parameters and Gaia photometry and astrometry (see de Laverny 2024, in preparation, for a detailed description). First of all, the E(Bp-Rp) extinction is estimated comparing the observed Gaia (Bp-Rp) colour to the theoretical one, derived from Casagrande et al. (2021) and using the *GSP-Spec* parameters. We then computed the stellar luminosity, adopting the geometric distances from Bailer-Jones et al. (2021). The stellar mass is finally derived from this luminosity, using the corresponding effective temperature and surface gravity. The associated errors were estimated by propagating the uncertainties on the parameters, photometry and distances, thanks to Monte-Carlo realisations.

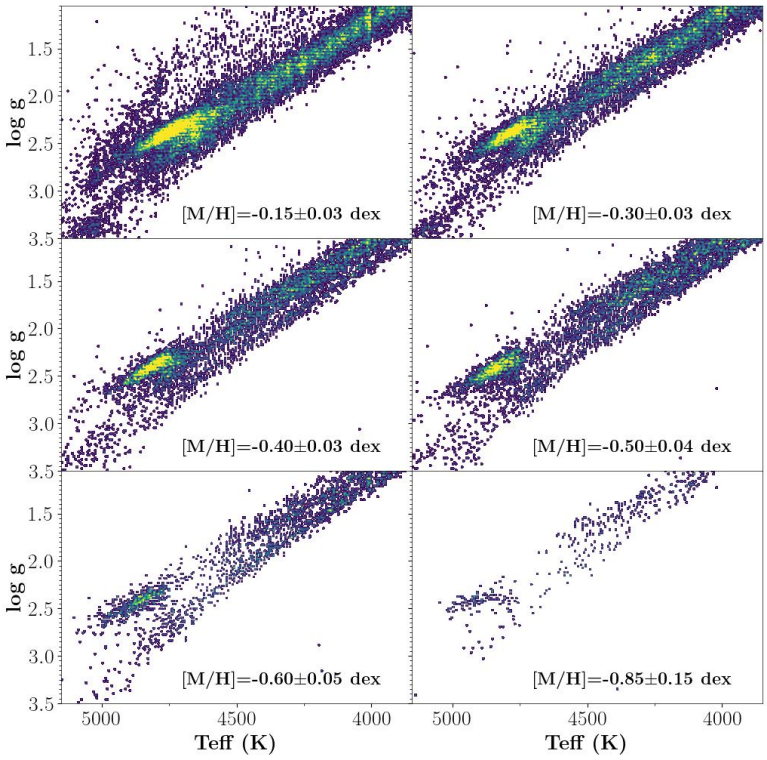

Fig. A.1. Density plot corresponding to Fig. 2 stellar populations.

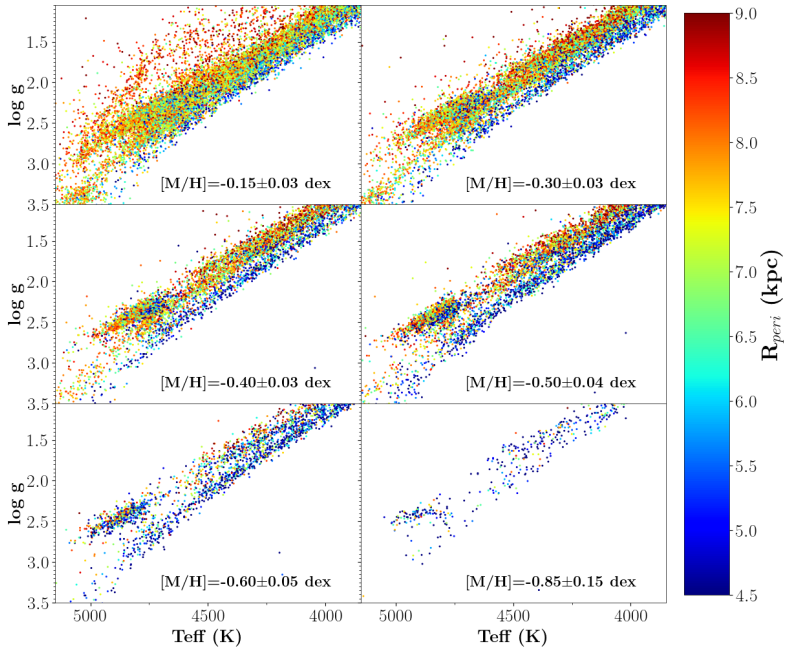

Fig. A.2. Same as Fig. 2, but colour-coded with the star orbital pericentre (R_{peri}).

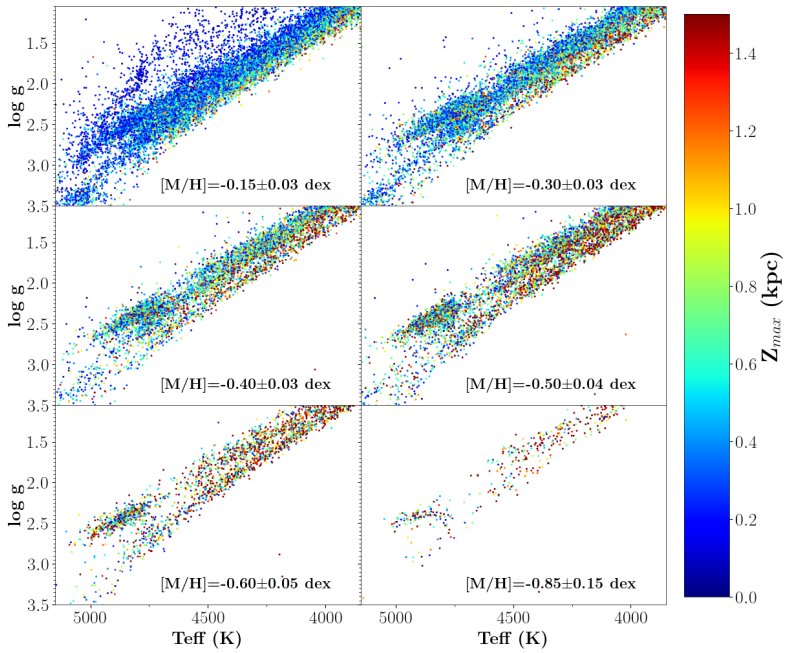

Fig. A.3. Same as Fig. 2, but colour-coded with star maximum orbital distance to the Galactic plane (Z_{max}), as a colour code.